Sensors & Actuators: A. Physical 366 (2024) 115002

Contents lists available at ScienceDirect

Sensors and Actuators: A. Physical

journal homepage: www.journals.elsevier.com/sensors-and-actuators-a-physical

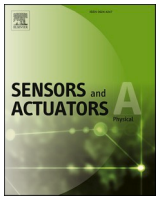

Piezoresistive relaxation and creep model of porous polymer nanocomposite supported by experimental data

Jianpeng Zhang [a], Ziya Wang [a], Chao Shang [a], Zhengfang Qian [a], Zhangming Wu [b], Xinge Yu [c], Zhengchun Peng [a,*]

[a] School of Physics and Optoelectronic Engineering, Shenzhen University, Shenzhen 518060, PR China
[b] School of Engineering, Cardiff University, Queen's Building, The Parade, CARDIFF CF24 3AA, Wales, UK
[c] Department of Biomedical Engineering, City University of Hong Kong, Hong Kong, China

ARTICLE INFO

Keywords:
Porous polymer nanocomposites
Piezoresistive sensor
Multi-mechanism modelling
Compressive relaxation behavior
Resistance creep

ABSTRACT

Porous piezoresistive nanocomposites (PPNs), a blend of conductive nanomaterials and a porous polymer matrix, have garnered significant attention in the realm of flexible pressure sensors. The porous microstructure offers exceptional sensitivity and lightweight characteristics of these sensors, but it also introduces challenges such as relaxation and creep behaviors. Grounded in viscoelastic theory, this paper introduces a mathematical model that provides a quantitative analysis of the resistance-strain relationship of PPN-based piezoresistive sensors, considering both bulk resistance and contact resistance. To elucidate the relaxation and creep behaviors, the model incorporates the conformational change and the slip motion of the polymer macromolecules during the deformation. Utilizing the Adam optimization algorithm, the model can accurately depict the piezoresistive behavior of various PPNs (with different porosities and conductive nanomaterial contents) with a fitting accuracy exceeding 99%. Furthermore, we explored some atypical characteristics of the PPN-based sensor, such as the negative resistance-strain behavior and the overshooting of bulk resistance. This study sets a theoretical basis for the development of sensitive and stable PPN-based sensors.

1. Introduction

Porous piezoresistive nanocomposites (PPNs), known for their unique electrical resistance properties that alter with mechanical deformations, have become a focal point in the field of smart-sensing applications[1–4]. These applications span a wide range, including pressure measurements[3], human-machine interfaces[4], healthcare [5], energy harvesting[6], flexible tactile sensors[7], biochemical systems[7], robotic devices[7], and more. To enhance the performance of PPNs, various foaming processes have been developed, such as batch foaming [8], extrusion foaming [9], and foam injection molding[10]. Additionally, a plethora of composite systems can be utilized to bolster the mechanical properties of PPNs. These include matrix materials like silicone rubber (SR) [11], polydimethylsiloxane (PDMS) [12], thermoplastic polyurethane (TPU) [13], and conductive fillers like carbon-based nanoparticles (e.g., Carbon black nanoparticles (CB)[14], Carbon nanofiber (CNF)[15], Carbon nanotube (CNT) [2], graphene nanoplatelets [16]) and conductive nanofibers (e.g., $BaTiO_3$ nanoparticles [17], metal nanoparticles [18]). When compared to solid piezoresistive nanocomposites (SPNs), PPNs exhibit several superior characteristics, such as excellent flexibility, stretchability, and high sensitivity, which can be attributed to the ability of PPNs to collapse voids [19,20].

Creating conductive networks within an insulating matrix is attributed to two factors: the direct contact between neighboring fillers providing an electron path, and the formation of quantum tunneling junctions between neighboring fillers within a certain distance[21,22]. The sensing mechanism of solid piezoresistive nanocomposites (SPNs) is explained by the tunneling effect, where resistance increases due to the loss of contact between neighboring fillers and the expansion of inter-filler distance[22,23]. Numerous superior insulating matrices have been proposed, particularly in terms of biocompatibility, super-elasticity, and ease of processing [24–26]. Notable examples include Poly(glycerol sebacate) (PGS) and Thermoplastic polyurethane elastomer (TPU). Over the past two decades, PGS, with its advantageous biocompatibility, super-elasticity, linear degradation profiles, and simple synthesis, has

* Corresponding author.
E-mail address: zcpeng@szu.edu.cn (Z. Peng).

https://doi.org/10.1016/j.sna.2023.115002
Received 20 March 2023; Received in revised form 22 December 2023; Accepted 31 December 2023
Available online 3 January 2024

been widely used in the field of soft tissue engineering to replicate the properties of soft tissues[25,27]. TPU, a heat-meltable and solvent-dissolvable material, is known for its unique molecular structure that facilitates easy processing, abrasion resistance, and superior elasticity [28]. Many studies have utilized TPU to enhance the lightweight, high compressibility, and high piezoresistive performance of PPNs [3,4,8,28,29]. By optimizing the tunneling effect, Wang et al. were able to fabricate an ultra-sensitive carbon black (CB)/TPU strain sensor with a gauge factor (GF) of 8962.7 at 155% strain and an adjustable scaffold network[28]. It's worth noting that theoretical models of SPNs have been proposed to explain their mechanical, electrical, and hysteresis behaviors[29–31]. In the model considering the tunneling effect, resistance is viewed as a series of connections of conductive fillers and a parallel connection of conducting paths [32]. The evolution of these conductive networks within the polymer matrix is time-dependent due to the internal friction between molecular chains. Therefore, akin to stress relaxation, the resistance relaxation of SPNs can be modeled using a generalized Maxwell model[29].

PPNs are known to have enhanced piezoresistive properties, such as increased sensitivity, improved flexibility, reduced modulus, and lighter weight compared to SPNs [20]. The presence of porous structures in PPNs reduces density, elevates electrical resistance, and aids in the alteration of conductive networks[24]. However, these varying conductive networks can result in complex piezoresistive behavior. For instance, SPNs typically display a positive piezoresistive property, meaning their resistivity decreases as pressure increases [33]. Conversely, PPNs can exhibit both positive and negative piezoresistive responses, depending on the foaming process and microstructure factors [20]. Key microstructural features, such as the homogeneity and interconnectivity of porous structures, pore size and distribution, and cell wall thickness, influence the pore collapse characteristics, which in turn alter the conductive networks in PPNs[34–36]. The common preparation methods for abundant microstructures primarily comprise sol-gel processing and templated methods [37]. PPN via sol-gel processing typically exhibits larger pore sizes, more uniform pore morphologies, and higher porosity rates, which are attributed to the chemical reactions and drying conditions involved in the sol-gel process[38]. In contrast, porous materials fabricated through templated methods enable precise control over pore sizes and structures based on the pore diameter and density of the template, offering enhanced tunability due to the flexible adjustment of template selection and design for tailoring the morphology and properties of the porous materials [28]. In addition to sol-gel processing and templated methods, other preparation techniques can be used to obtain more abundant PPNs, such as freeze-drying, phase separation, 3D printing, and emulsion templating [39–41]. As a result, an interconnected porous structure can exhibit high sensitivity and robust cyclic response under a low strain range, while hierarchical pore structures can enable a wide range of linear behavior[28,42]. The resistance-strain behaviors of a graded nest-like PPN display a piecewise linear characteristic, approximately within the range of two GFs, under compression or stretching due to initial sensitivity from the tunneling effect in the cell wall[43]. High GFs in large deformation will be developed for 3D printing PPN from collapsing cell structures[35]. However, in PPNs, the interplay between molecular conformational changes, microscale motion of polymer macromolecules, deformation of the porous matrix, and pore collapse presents significant challenges in developing accurate theoretical/numerical models. In our previous work, we proposed a quasi-static theoretical piezoresistive model of hierarchical PPNs, considering both the tunneling effect and the collapsing effect of the microporous structure[23]. The limitations of this model include low-precision bulk resistance, a narrow application range, and the absence of a dynamic term. Furthermore, the presence of strain concentration in the porous structure adds complexity to resistance-strain behaviors, relaxation behaviors (the change of the resistance value over time after a rapid change in the driving compressed deformation applied to the material), and creep behavior (the change of resistance value over time after the stress or pressure is removed) [30,31,44]. Prior studies on the cyclic piezoresistive performance of PPNs have shown that ideal dispersion of conductive fillers and a remarkably uniform cell structure morphology can provide excellent strain-dependent sensitivity and repeatability [29]. However, there is currently a lack of analytical models that can accurately analyze the mechanism of piezoresistive response behaviors and piezoresistive hysteresis phenomenon, which hinders the design and application of PPN sensors.

In this study, we propose and establish a mathematical model that takes into account the resistance-strain relationship, resistance relaxation, and creep behavior of PPNs. We modify Ogden's incompressible hyper-elastic model by introducing a compressible energy term, allowing us to study the compressive hyper-elastic behaviors of PPNs [45]. Additionally, we employ a generalized Maxwell model to simulate the viscoelastic behaviors of PPNs [32]. We also develop a simplified resistance-elongation model that considers all potential factors, including tunneling and geometrical effects. By examining the correlation between changes in the conductive network and the disorientation of polymer macromolecules, we propose a quasi-static piezoresistive model. By integrating this model with the Maxwell model, we establish relaxation and creep models for PPNs' resistance. To validate these analytical models, we conduct a series of experiments on different PPN-based sensors using varying compression amplitudes and speeds during the test. Furthermore, we use the Adam (Adaptive Moment Estimation) neural network optimization algorithm, known for its high accuracy and rapid convergence, to fit these experimental results. The key parameters obtained from the Adam algorithm can be used to guide the design of the PPNs.

1.1. Analytical modelling

1.1.1. Mechanical model

As PPNs are well-known for their high compressibility and the decrease in volume with increasing pressure, they exhibit excellent cyclic performance and stable piezoresistive properties due to their compressible cell structures and the desired dispersion of conductive fillers throughout the porous media. Using the modified Ogden model (see Supplementary Materials, S1.1), the principal stresses of PPNs under uniaxial compression can be determined as

$$\sigma = \frac{1}{\lambda}\sum_{i=1}^{n}\frac{2\mu_i}{\alpha_i}\left(\lambda^{\alpha_i} - J^{-\alpha_i\beta_i}\right) \tag{1}$$

where λ is the primary elongation, α_i and μ_i $(i = 1,2,3,\ldots,n)$are material parameters,Jdenotes the volume ratio. When compressing a PPN, there are three constraint conditions to describe the volume ratio

$$\begin{cases} J = 1, \lambda = 1 \\ \dfrac{\mathrm{d}J}{\mathrm{d}\lambda} = 1, \lambda = 1 \\ J = p, \lambda \to 0 \end{cases} \tag{2}$$

Thus, the volume ratio can be assumed as

$$J = (1-p)e^{1/(1-p)} + p \tag{3}$$

where p is the relative density of PPN.

1.1.2. Bulk resistance model

The electrical properties of PPNs mainly depend on conducting fillers, which are dispersed within insulating matrices to form pore walls. Considering that the behaviors of a single tunnel junction can reasonably describe the conductivity of a composite solid (Figs. 1e, 1f, and 1g), an approximate model [46] is proposed to describe its conducting behaviors as,

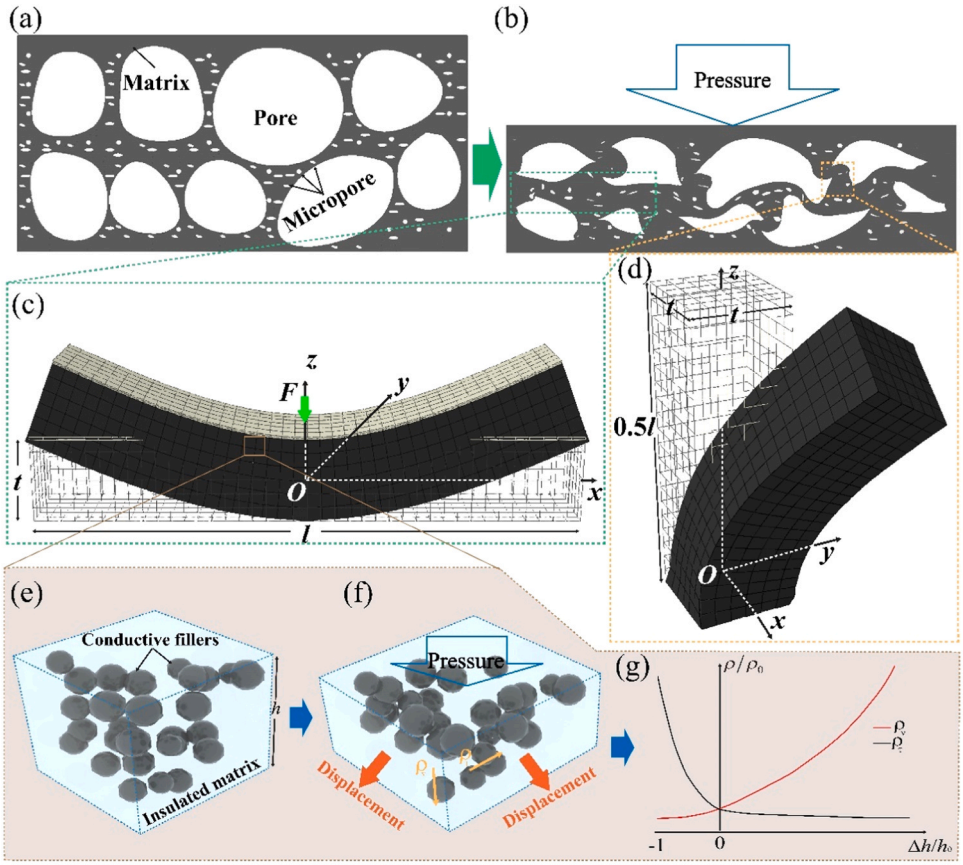

Fig. 1. Generation of the piezoresistive performance based on tunneling effects and geometric effects. Schematic of a PPN (**a**), and the compressed PPN (**b**). Schematic view of the simple supporting beam (**c**) and pure bending beam (**d**) within the PPN. (**e**), Schematic of composite solid with conductive particles. (**f**) Compression deformation of the composite solid to demonstrate the change of distance between conductive particles. (**g**) The curves of resistivity with strain at different directions.

$$\rho = \rho_0 e^{2Xd_0\varepsilon}/p = \rho_0 e^{2mX}/\sqrt[3]{V_s p\varepsilon}/p \tag{4}$$

where$X = \sqrt{2rV(T)}/h$, ρ_0 is the resistivity of conductive fillers, r is the mass of charge carriers, $V(T)$is the function of the temperature-dependent barrier height, m is a proportional constant. $d_0 = m(V_s p)^{-1/3}$,$V_s$is the volume fraction of the conductive fillers, and $p$is the relative density (the density of substrate materials against the density of its solid matrix) of PPN. The beam model is usually applied to analyze various properties of PPNs. According to Euler–Bernoulli theory (Supplementary Materials. S1.2), the resistances of transversely and vertically bent beams, as shown in Figs. 1c and 1d, respectively, are determined by,

$$R_{sq} = R^0_{sq}\left[1 - \sum_{i=1}^{n} A_i (C\lambda^n)^i\right] \tag{5}$$

where R^0_{sq} is the initial resistance, $A_i (i = 0, 1, 2, 3, .)$ are polynomial coefficients on the sensitivity to forces and C is the conductive parameter of doped composites. According to Archie's empirical model [47], the resistance of a PPN depends on its porosity of PPNs, as

$$R^0_{sq} = R^*_0 p_0^{-\varphi} \tag{6}$$

where $R^*_0 \propto e^{2Xm\phi^{-1/3}}$ is the resistance of SPNs and $\varphi \in (1, \infty]$is the topological constant to describe the closure of micro-pores, as shown in Figs. 1a and 1b. Therefore, considering the geometrical effect based on the effective medium theory, the resistance is calculated as,

$$R' = R^0_{sq}\lambda_1^{\varphi} J^{2\varphi} \tag{7}$$

However, the above expression of bulk resistance is too complex to analyze the piezoresistive effect. Therefore, the given equation is simplified to the following form,

$$\frac{R^s_{sq}}{R^0_{sq}} = \frac{\left(A\lambda^a + (1-A)J^b\right)}{\lambda} \tag{8}$$

where $1/\lambda$is due to the decrease of sectional areas, A and a are terms from bending pore walls (S1.2), $(1 - A)$and b are terms representing the closure of pore.

1.1.3. Contact resistance model

Figs. 2a and 2b schematically show the interfacial topologies between porous nanocomposites and electrodes. The partially magnified interfacial topologies are shown in Figs. 2c and 2d, which demonstrate the change of contact characteristics. There are mainly two types of features changing: increasing contact resistance from the slippage at the interface; and decreasing resistance from the increase of contact areas. According to the quantitative electrical contact resistance (ECR) theory [48], the ECR (R_c) is given by,

$$R_{con} = \frac{\rho}{\sqrt{\pi A_{eq}}}\left[(1-B) + B\lambda^{-d}\right] \tag{9}$$

where $A_{eq} \approx A_{eq0} J^{-\frac{2}{3}c}$is the equivalent contact area between electrodes and PPNs, $B(B > 0)$and $c(c > 0)$ represent the increase of the effective conducting contact areas, and d represents the reconstructed conductive

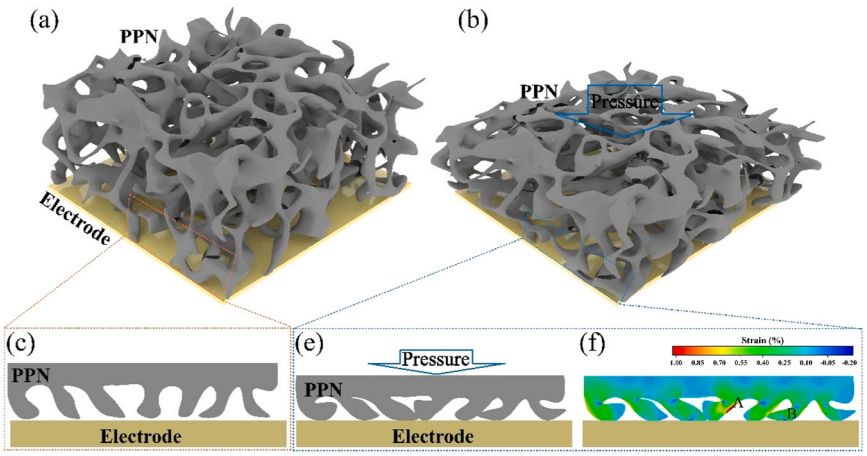

Fig. 2. Schematic showing the characteristics of interfacial contact between porous composite and electrodes. (**a**) Interfacial contact structure with partial magnified drawing (**c**) and (**b**) its compression deformation under pressure with partial magnified drawing (**d**). (**e**) Strain contour of the interfacial structure with point *A* and point *B*.

paths from slipping contact areas. Thus, the ECR (R_c) can be rewritten as

$$R_{con} = \frac{\rho}{\sqrt{\pi A_{eq0}}} J^{\frac{\xi}{3}} \left[(1-B) + B\lambda^{-d}\right] \tag{10}$$

Taking the volume fraction of the conductive fillers (V_s) and relative density (p), the original contact resistance (R^0_{con}) can be proposed as

$$R^0_{con} = \frac{\rho_0 e^{2mX/\sqrt[3]{V_s p}} V_s^{\,n} \left(y_c + k(p-p_c)^6\right)}{p\sqrt{\pi A_e}} \tag{11}$$

where A_e is the equivalent contact area between electrodes and conductive fillers, $n$is constant representing the influence of the volume

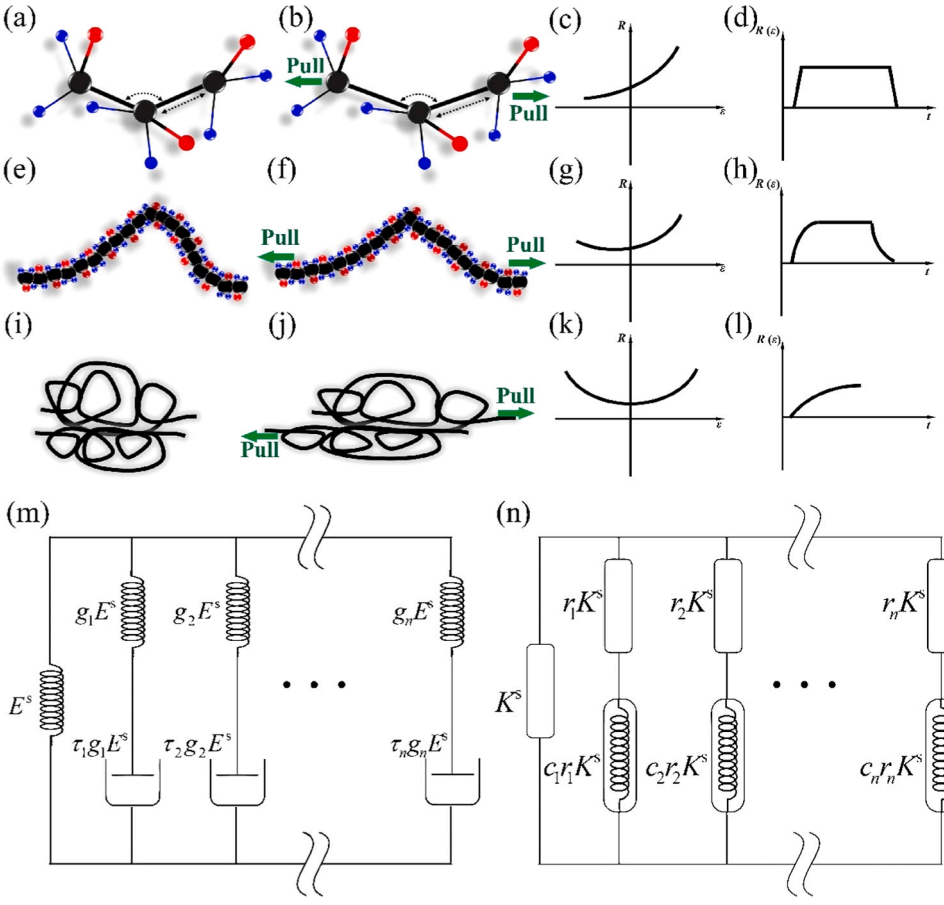

Fig. 3. Schematic showing the domain of the piezoresistive relaxation model. Schematic diagram and deformation of bond angle and length (**a, b**), segmental motion (**e, f**) and relative slippages between molecular chains (**i, j**). The resistance curves of bond angle and length (**c**), segmental motion (**g**) and relative slippages between molecular chains (**k**) change with strain. The resistance (strain) relaxation curves along with the time of bond angle and length (**d**), segmental motion (**h**) and relative slippages between molecular chains (**l**). (**m**) The generalized Maxwell model of the mechanical viscoelastic behaviors with $E = \partial\sigma/\partial\varepsilon$ as modulus. (**n**) Representation of the resistance relaxation model of PPNs with $K = \partial R/\partial\varepsilon$ as sensitivity to deformation.

fraction of the conductive fillers (V_s) on contact conditions, y_c, k and p_c are offset, width and center of the contact function resulting from synthetic effects of porous structure at the interface.

1.2. Piezoresistive relaxation model

The time- and rate-dependent piezoresistive behaviors of PPNs are analyzed using a piezoresistive relaxation model that takes into account both the hyper-viscoelastic and resistance relaxation properties of PPNs. According to polymer physics [49], there are three kinds of changes on the molecular scale that produce the deformation of polymer composite. The change of bond lengths and bond angles produces elastic deformation that satisfies exponential correlation with resistance ($R \propto e^{2Xd\varepsilon}$), and its state transition requires a short time (Figs. 3a, 3b, 3c, and 3d). Then, segments of molecular chains gradually move and rearrange to achieve high elastic deformation and state transition of the deformation follows exponential correlation with time ($\varepsilon = \varepsilon_0(1 - e^{-t/\tau})$), as shown in Figs. 3e, 3f, 3g, and 3h. Furthermore, relative slippages between molecular chains happen under bigger deformation, as shown in Figs. 3i and 3j. This deformation will destroy conductive paths increasing resistance (Fig. 3k) and it has no spontaneous elastic recovery (Fig. 3l). The above results reveal the relationship between creeping strain and creeping resistance at the molecular level. To describe the mechanical relaxation behaviors of polymeric material based on the above phenomena, a generalized Maxwell model is established and its graphical representation is shown in Fig. 3m [32]. Based on the dependency between deformation and resistance (Eq. 4), a resistance relaxation model similar to the generalized Maxwell model is performed in Fig. 3n. When a uniaxial loading is applied on the PPNs, the relaxation response can be obtained as,

$$\begin{cases} \sigma(t) = \sigma^s(t) - \sum_{i=1}^{N} \frac{g_i}{\tau_i} \int_0^t (\sigma^s(t-s) - \sigma^s(t)) e^{-s/\tau_i} ds \\ \frac{R_{sq}}{R_{sq}^0}(t) = \frac{R_{sq}^s}{R_{sq}^0}(t) - \sum_{i=1}^{N} \frac{g_i^r}{\tau_i^r} \int_0^t \left(\frac{R_{sq}^s}{R_{sq}^0}(t-s) - \frac{R_{sq}^s}{R_{sq}^0}(t) \right) e^{-s/\tau_i^r} ds \\ \frac{R_{con}}{R_{con}^0}(t) = \frac{R_{con}^0}{R_{con}^0}(t) - \sum_{i=1}^{N} \frac{g_i^c}{\tau_i^c} \int_0^t \left(\frac{R_{con}^0}{R_{con}^0}(t-s) - \frac{R_{con}^0}{R_{con}^0}(t) \right) e^{-s/\tau_i^c} ds \end{cases} \quad (12)$$

g_i and τ_i are the i-th relative modulus and relaxation time of stress, g_i^r and g_i^c are the relative relaxed resistance for bulk resistance and contact resistance, respectively. τ_i^r and τ_i^c is the i-th relaxation time of bulk resistance and contact resistance, respectively,

After releasing the pressure on the PPN, the resistance starts to recover. Thus, the creep of the recovered resistance can be described as,

$$\begin{cases} M_\lambda = \lambda(t_1)^{a-1} - \sum_{i=1}^{N} \frac{g_i^r}{\tau_i^r} \int_0^{t_1} \left[\lambda(t_1 - s)^{a-1} - \lambda(t_1)^{a-1} \right] e^{-s/\tau_i^r} ds \\ H_J = J(t_1)^{\frac{c}{3}} - \sum_{i=1}^{N} \frac{g_i^c}{\tau_i^c} \int_0^{t_1} \left[J(t_1 - s)^{\frac{c}{3}} - J(t_1)^{\frac{c}{3}} \right] e^{-s/\tau_i^c} ds \\ M = J(t_1)^b \lambda(t_1)^{-1} - \sum_{i=1}^{N} \frac{g_i^r}{\tau_i^r} \int_0^{t_1} \left[J(t_1 - s)^b \lambda(t_1 - s)^{-1} - J(t_1)^b \lambda(t_1)^{-1} \right] e^{-s/\tau_i^r} ds \\ H = J(t_1)^{\frac{c}{3}} \lambda(t_1)^{-d} - \sum_{i=1}^{N} \frac{g_i^c}{\tau_i^c} \int_0^{t_1} \left[J(t_1 - s)^{\frac{c}{3}} \lambda(t_1 - s)^{-d} - J(t_1)^{\frac{c}{3}} \lambda(t_1)^{-d} \right] e^{-s/\tau_i^c} ds \end{cases} \quad (14)$$

$$\begin{aligned} \frac{R_{sq}}{R_{sq}^0}(t) &= A\left(1 - \sum_{i=1}^{n} \phi_i^\lambda [1 - M_\lambda] e^{-t/s_i^\lambda}\right) + (1 - A)\left(1 - \sum_{i=1}^{n} \phi_i [1 - M] e^{-t/s_i}\right) \\ \frac{R_{con}}{R_{con}^0}(t) &= (1 - B)\left(1 - \sum_{i=1}^{n} \theta_i^J [1 - H_J] e^{-t/c_i^J}\right) + B\left(1 - \sum_{i=1}^{n} \theta_i [1 - H] e^{-t/c_i}\right) \end{aligned} \quad (13)$$

where t_1 is compression duration,

are variations during compression for strain, volume strain, and their coupling. s_i^λ,c_i^J,s_i and c_i are the i-th creep time for them. $\sum_{i=1}^{n} \phi_i^\lambda = 1$,$\sum_{i=1}^{n} \theta_i^J = 1$,$\sum_{i=1}^{n} \phi_i = 1$ and $\sum_{i=1}^{n} \theta = 1$ are the i-th creep resistance for them.

All the above relaxation parameters including mechanical parameters and electrical parameters are difficult to determine by experiments. Therefore, with the representative data collected from experiments, a machine learning method (Adam optimization algorithm in Supplementary Materials.S5) is applied to determine the relaxation parameters.

2. Results and discussion

2.1. Piezoresistive relaxation behaviors of PPNs

A PPN sample is created using the salt leaching technique method (see Supplementary Materials.S2) [50–52]. The SEM images of the microstructures of this PPN sample are provided in Fig. 4. Three typical pores, denoted by a yellow dotted line, are observed (Figs. 4b and 4c). Large pores, approximately 50 μm in size, are formed from clusters templating of inorganic salt (Fig. 4b). Middle-sized pores, around 10 μm, are primarily derived from inorganic salt monomer templating (Fig. 4c). Small pores, about 1 μm, are identified from the aperture gaps between inorganic salt monomers due to the volatilization of organic solvents (Fig. 4e). CB nanoparticles doped in the wall of the micropores structures of the PPN form crosslink conductive networks (Fig. 4d), which are susceptible to the deformation of the pore wall. Several sensor samples are created to study the piezoresistive behaviors of PPN using an experimental measurement system (see Supplementary Materials S2 & Fig. S3). The measurement of contact resistance applies the difference between 2-wire resistance and 4-wire resistance with structural parameter correction (Fig. S4).

Fig. 5 displays the effects of CB content and relative density on the bulk resistance and contact resistance of PPNs. Using the fitted equations provided in Eqs. (4) and (11), the experimental data were analyzed and key parameters were determined (see Table S1 for details). The resistance data in Figs. 5a and 5c indicate that increasing CB content within the PPNs (1-p, 70% porosity) enhances the conductive paths both within the polymer matrix and at the electrode-PPN interface, resulting in a

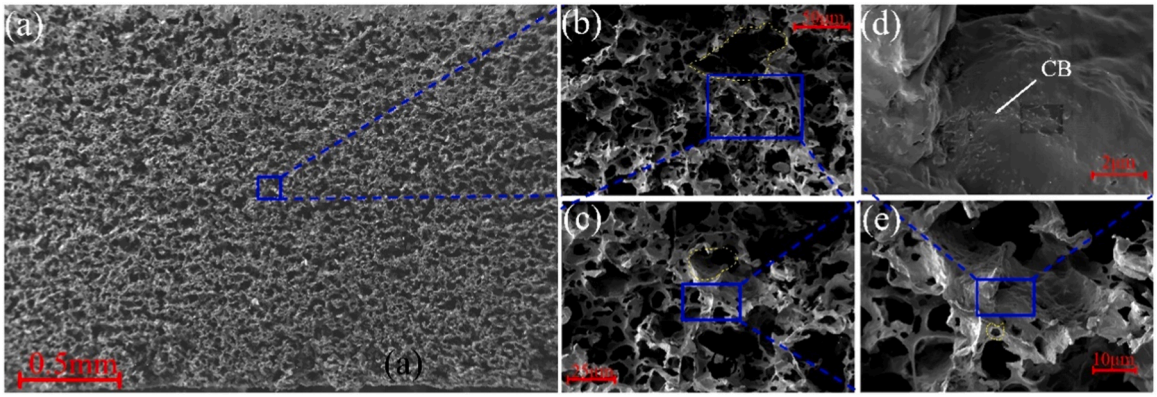

Fig. 4. (a-e) SEM morphology of CB/TPU foam (15 wt% CB and 500 wt% dosage of IST).

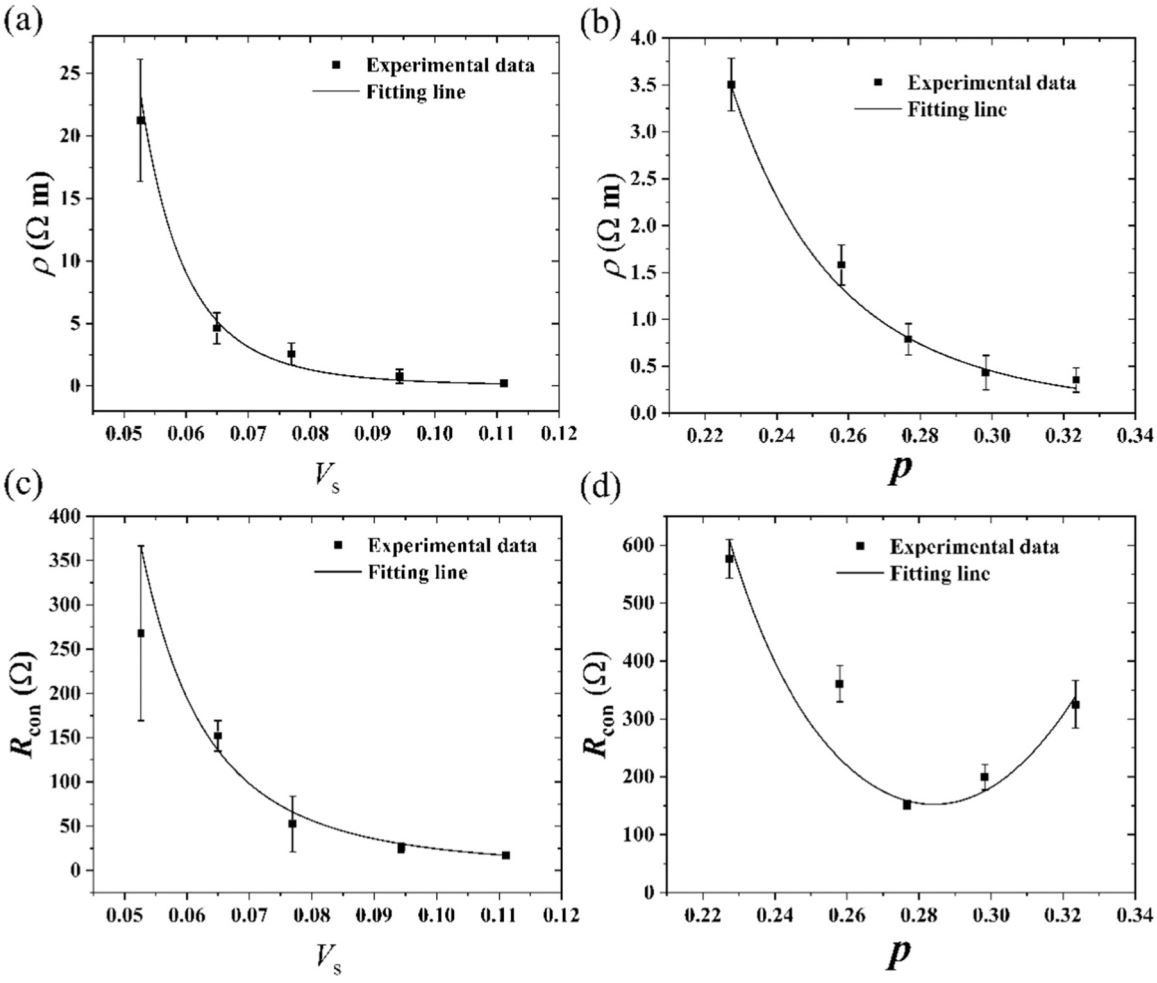

Fig. 5. Effect of CB content ($p = 0.298$) and relative density (V_s=0.095) on bulk resistance and contact resistance. Experimental data and fitting line of bulk resistance depended on CB content (**a**) and relative density (**b**). Experimental data and fitting line of contact resistance depended on CB content (**c**) and relative density (**d**).

reduction of resistivity. Similarly, Fig. 5b shows that increasing relative density within the PPNs (9.5 wt% CB content) also enhances the conductive paths within the polymer matrix. However, the effective contact area between the electrode and PPN is influenced by both the porosity and hardness characteristics of the PPN. As relative density increases, porosity decreases, which may lead to an increase in contact area due to improved mechanical interlocking between the electrode and PPN [53–55]. However, simultaneously, an increase in the relative density of PPNs (9.5 wt% CB content) also leads to an increase in interface hardness, which may counteract the increase in contact area. Therefore, the fitted line in Fig. 5d exhibits a non-monotonic trend, showing a decrease in contact resistance at first, followed by an increase. These findings suggest that both CB content and relative density have significant effects on the piezoresistive behavior of PPNs, with complex interactions between various factors contributing to the overall resistance characteristics.

A series of experiments were conducted to investigate the piezoresistive behaviors of PPN (75% porosity and 15 wt% CB content) using a controlled sample preparation and testing protocol. To assess the piezoresistive characteristics of PPN under investigation, a specimen with dimensions measuring 10 × 10 × 1 mm was precisely positioned within a planar four-electrode apparatus (Fig. S3). Utilizing a controlled press machine, the specimen underwent a uniform compression process at a standardized rate of 5 mm/min, attaining a compression ratio of 75%. This compressive state was maintained for a duration of 300 s to meticulously observe the resistance relaxation behavior within the material. Subsequently, the compression was swiftly released, allowing the specimen to revert to its original form over a monitoring period of another 300 s, while continuously recording any alterations in electrical resistance. This methodological approach ensures a rigorous and scientific evaluation of the piezoresistive properties exhibited by the porous material. The quasi-static piezoresistive characteristics, including stress (Fig. 6a), bulk resistance (Fig. 6b), and contact resistance (Fig. 6c), were measured and analyzed. The experimental results indicate that effective modulus (E^s) and sensitivity to deformation (K^s) increase with the deformation of PPN due to the closure of pores and wall buckling of micropores. Unexpectedly, the contact resistance increases at the initial compression stage due to slippage at the interface, disrupting the conductive paths (as shown in Fig. 2). Subsequently, the relaxation curves of stress and resistance exhibit a similar slow downward trend in Figs. 6d, 6e, and 6f. This trend is attributed to the internal friction within the molecular chains and segmental motions within the matrix of PPN. Furthermore, Figs. 6g, 6h, and 6i illustrate the creep behavior exhibited by both stress and resistance during the decompression of the compressed PPNs. The stress curve is initiated at a pre-pressure of 1kPa. The recovery of contact resistance follows the trend of strain recovery, with both exhibiting a gradual return to their initial values. However, the bulk resistance at the creeping stage exceeds the initial value ($R_{sq}/R^0_{sq} > 1$) due to relative slippages between molecular chains under large deformation, which require more time to recover than the recovery time of molecular bond variations and segmental motions ($s_1^{\lambda} = 2.79\text{s} << s_1 = 102.09\text{s}$). The mathematical model developed in this study exhibits good agreement with experimental results ($R^2 > 0.99$), providing key parameters (see Table 1 for detail) to accurately define piezoresistive characteristics of PPNs

The relaxation behaviors of PPNs are described using the analytical model that includes two main components: molecular bond variation and segmental motion. These behaviors are characterized by short-term

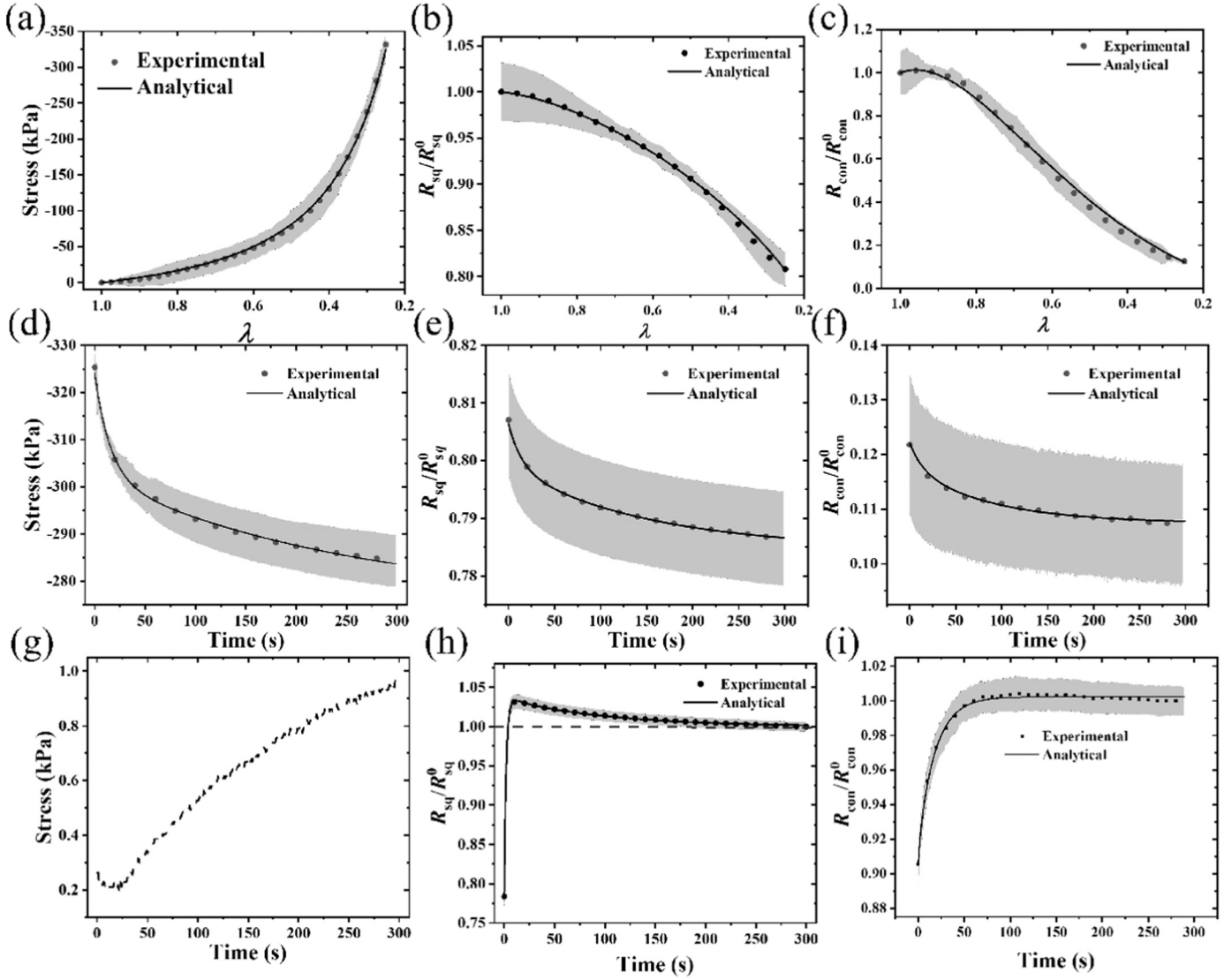

Fig. 6. Measured and modelled piezoresistive response vs. stretch curve and piezoresistive relaxation response vs. time curve. The general characteristics of piezoresistive stress **(a),** piezoresistive bulk resistance **(b)** and piezoresistive contact resistance **(c)**. The relaxation behaviors of stress **(d)**, bulk resistance **(e)** and contact resistance **(f)**. The creep response of stress **(g)**, bulk resistance **(h)** and contact resistance **(i)**.

Table 1
Piezoresistive parameters of the PPN sensor.

	Quasi-static			Relaxation				Creep			
Stress	μ(kPa)	α	β	g_1	g_2	τ_1(s)	τ_2(s)				
	14.493	1.943	0.8085	0.2810	0.2287	7.8877	118.06				
Bulk resistance	A	a	b	g_1^r	g_2^r	τ_1^r(s)	τ_2^r(s)	ϕ_1^λ	ϕ_2^λ	s_1^λ(s)	s_2^λ(s)
	1.1392	1.2033	1.9276	-0.4898	-0.5057	4.8628	282.59	0.6133	0.3867	2.7874	1.2874
								ϕ_1	ϕ_2	s_1(s)	s_2(s)
								0.3729	0.6371	6.6364	102.09
Contact resistance	B	c	d	g_1^c	g_2^c	τ_1^c(s)	τ_2^c(s)	θ_1^I	θ_2^I	c_1^λ(s)	c_2^λ(s)
	10.8575	13.0580	0.4864	-0.868	-0.0911	5.8155	113.98	1.0377	-0.377	6.6835	1.6062
								θ_1	θ_2	c_1(s)	c_2(s)
								0.9884	0.0116	6.7138	56.0632

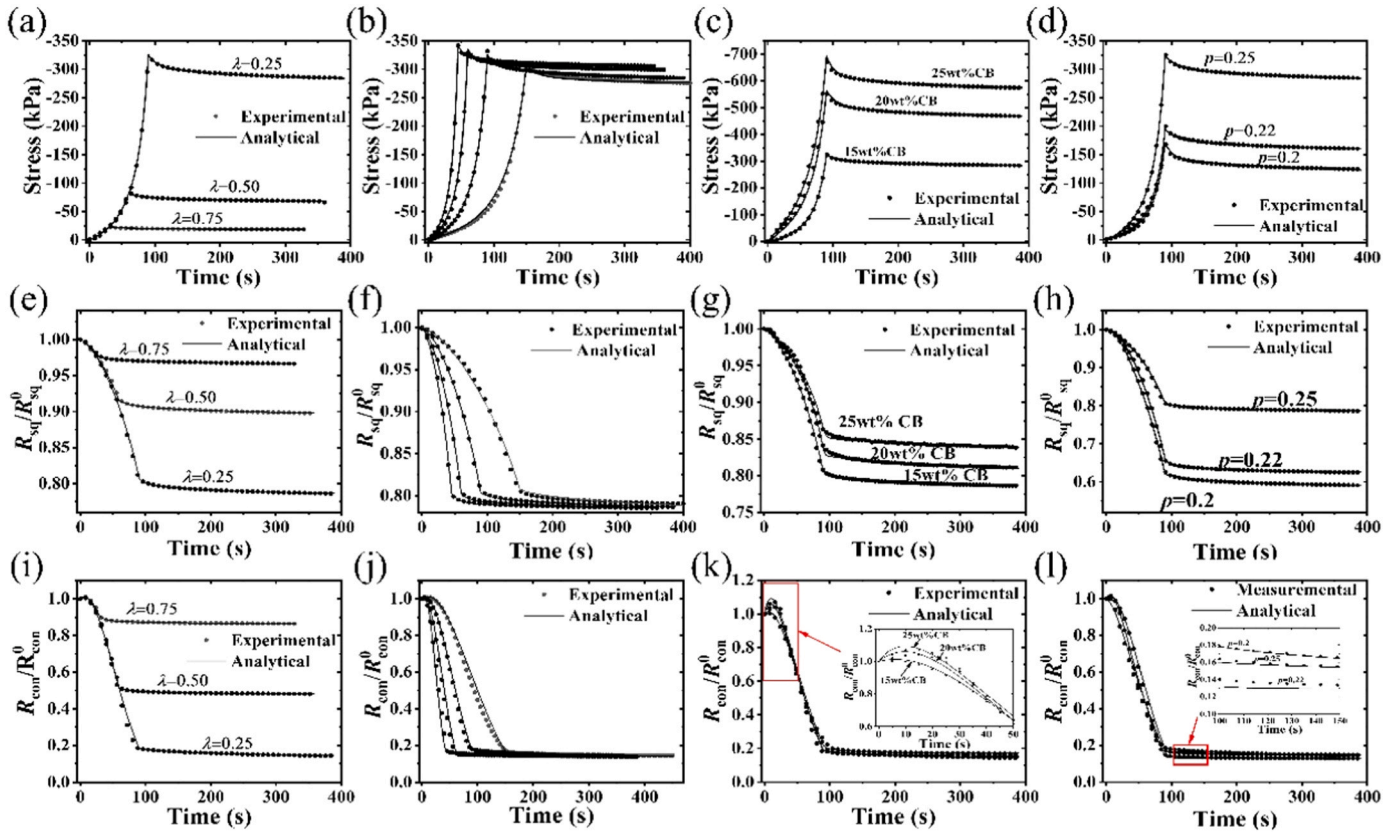

Fig. 7. Mechanical and piezoresistive relaxation responses, as well as relaxation parameters of PPN sample in case of compressive relaxation test performed at λ = 0.25,0.50 and 0.75 (p = 0.25 and V_s= 9.5 v%) **(a, e and i)**, at speed= 0.30, 0.50, 0.75 and 1.00 mm/min (p = 0.25 and V_s= 9.5 v%) (**b, f and j**), at different CB content (p = 0.25)(**c, g and k**), at different relative density (V_s= 9.5 v%) (**d, h and l**).

($g_1$andτ_1) and long-term parameters ($g_2$andτ_2), which reflect internal friction of molecular bond change and segmental motion, respectively. The fitting results (Fig. 7) indicate that the short-term parameters τ_1 ($1 \sim 7$s),τ_1^r ($4 \sim 6$s) and τ_1^c ($3 \sim 7$s), which are related to the internal friction of molecular bond changes, are significantly smaller than the long-term parameters τ_2($70 \sim 120$s),τ_2^r($70 \sim 400$s) and τ_2^c($70 \sim 250$s), which represent segmental motion. Furthermore, the results indicate that the long-term relaxation time of bulk resistance is greater than that of contact resistance. This suggests that contact signals may provide a more rapid response to pressure detection. Based on previous research on solid conductive composites, it has been found that increasing tensile amplitudes and speeds can lead to an increase in the interparticle distance of the conducting fillers, resulting in a significant resistivity peak [32,56,57]. The results presented in Figs. 7a, 7e, and 7i further support this finding, showing that an increase in deformation amplitude leads to an increase in response amplitude but a reduction in relaxation time (Table S2). Additionally, an increase in loading speed (Figs. 7b, 7f, and 7j) tends to increase relaxation time (Table S1). When considering the effect of CB content in PPN, it is observed that an increase in CB content leads to an increase in effective modulus (Fig. 7c). However, it decreases the sensitivity of bulk resistance to deformation (Fig. 7g) and has a smaller influence on the sensitivity of contact resistance to deformation (Fig. 7k). Similarly, an increase in the relative density of PPN (Figs. 7d, 7h, and 7l) exhibits a similar trend concerning its CB content. The results indicate that the sensitivity of contact signal to deformation is relatively robust to composite content. Recent studies have also produced similar results [58–60]. However, some special responses depend on the application, such as the increase observed at the initial compression stage (Fig. 7k). It is worth noting that the increase can worsen with an increase in CB content.

The relaxation and creep behavior of PPNs, as shown in Figs. 8 and 9, is a complex phenomenon that involves positive terms (increasing the electrical resistance) and negative terms (decreasing the electrical resistance) in a piezoresistive Eq. (13). In the relaxation model, the

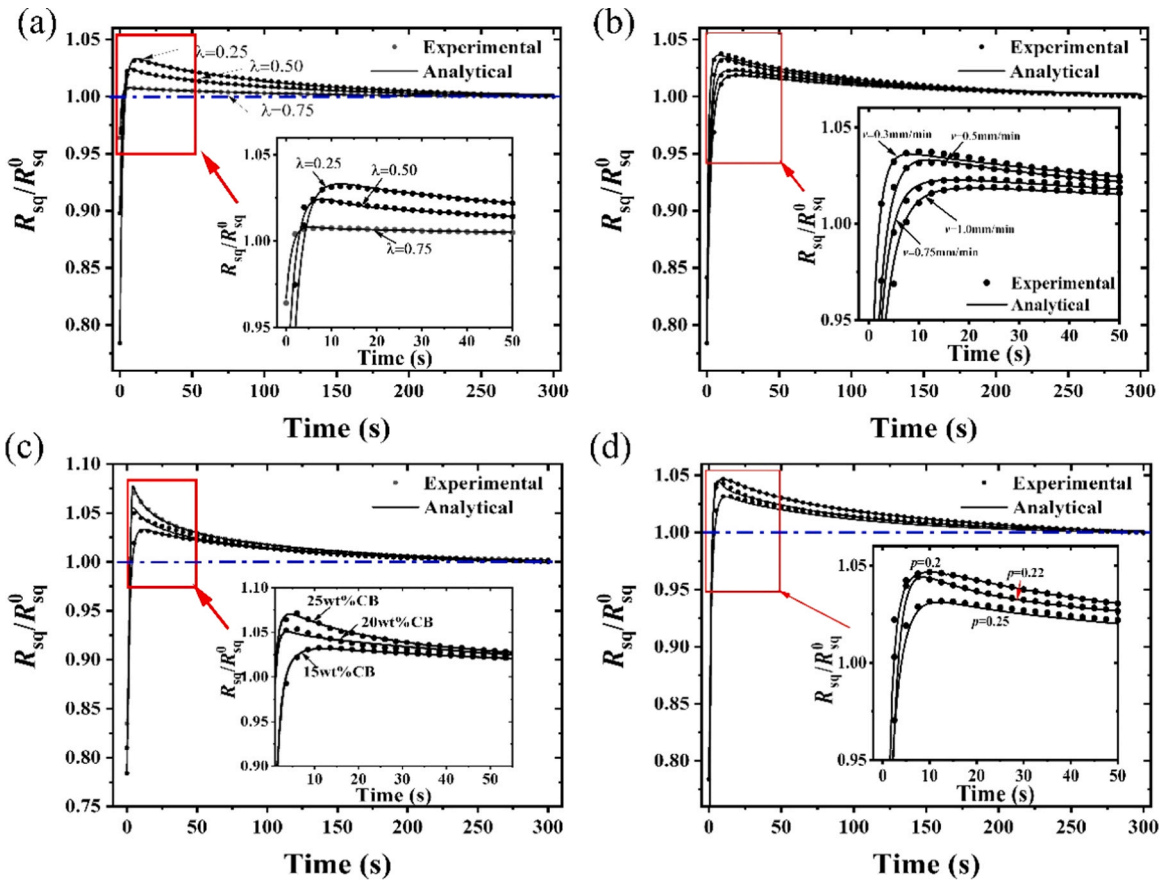

Fig. 8. Creep behaviors of bulk resistance under releasing conditions. Experimental data and analytical line of creep bulk resistance with compression amplitude ($p = 0.25$ and V_s= 9.5 v%) (**a**), compression speed ($p = 0.25$ and V_s= 9.5 v%) (**b**), CB content ($p = 0.25$) (**c**) and relative density (V_s= 9.5 v%) (**d**).

short-term parameters are responsible for the decrease in electrical resistance, while the long-term parameters lead to an increase in resistance. This increase may be attributed to the slippage of the molecular chains within the matrix of the PPN. Compression amplitude and compression speed are two key factors that distinguish the behavior of short-term and long-term parameters. When compression amplitude increases (Fig. 8a), the overshooting of bulk resistance also increases, indicating a more significant positive piezoresistive effect. Similarly, an increase in CB content (Fig. 8c) also leads to an increase in the overshooting value of bulk resistance. On the other hand, a decrease in compression speed (Fig. 8b) and relative density (Fig. 8d) results in a decrease in the overshooting value of bulk resistance, indicating a more significant negative piezoresistive effect. The uncommon creeping curve of bulk resistance shown in Fig. 8 suggests that the overshooting value is higher than the initial value. This behavior can be attributed to the interplay between various factors such as molecular chain slippage, microstructural changes, and interface effects within the material. The creeping curves of contact resistance in Fig. 9 demonstrate that the resistance gradually recovers to its original value over time. Fig. 9a indicates that the recovery time increases with compression deformation, likely due to the yield of the pore wall at the interface. In contrast, increasing compression speed has minimal impact on the recovery (Fig. 9b). Furthermore, the creep time of contact resistance (c_i) is shorter than that of bulk resistance (s_i) (Table S3), highlighting the practicality of contact resistance in PPN. Fig. 9c and d demonstrate that the recovery speed increases with an increase in CB content and a decrease in relative density. This can be attributed to a reduction in adhesion at the interface, where increasing CB content and porosity can enhance adhesion, resulting in a longer recovery time [61–64]. These findings provide valuable insight into the behavior of contact resistance of PPN, its response to various factors, and its practicality for applications. Understanding these behaviors is crucial for the development of piezoresistive materials with improved performance and reliability in various applications.

3. Conclusion

The analytical model proposed in this paper simulates and analyzes several piezoresistive behaviors of PPNs, taking into account both the tunneling effect of conductive fillers within the matrix and geometrical effects based on the effective medium theory of porous topology. The bending of pore walls and strain concentration in compressed PPNs not only result in compressive strain that decreases electrical resistance but also tensile strain that increases electrical resistance. The change in macromolecular chains upon compression of PPNs may lead to relaxation and creep behaviors of electrical resistance (bulk resistance and contact resistance). The increase in slippage between molecular chains can result in an overshooting of the bulk resistance once the compression is released. We also observed that decreasing CB content and relative density can increase the sensitivity of PPNs to deformation, and the contact resistance exhibits greater robustness in sensitivity to deformation, as well as faster response and recovery time compared to bulk resistance. By fitting several experimental results obtained under different loading conditions and using different composite systems, our analytical model reveals that two factors, i.e., molecular bond variation and segmental motion, determine the piezoresistive response, the relaxation behavior, and the creep of contact resistance and bulk resistance.

This analytical model is suitable for describing compressible PPNs, and offers a valuable tool for guiding the design of PPN sensors with

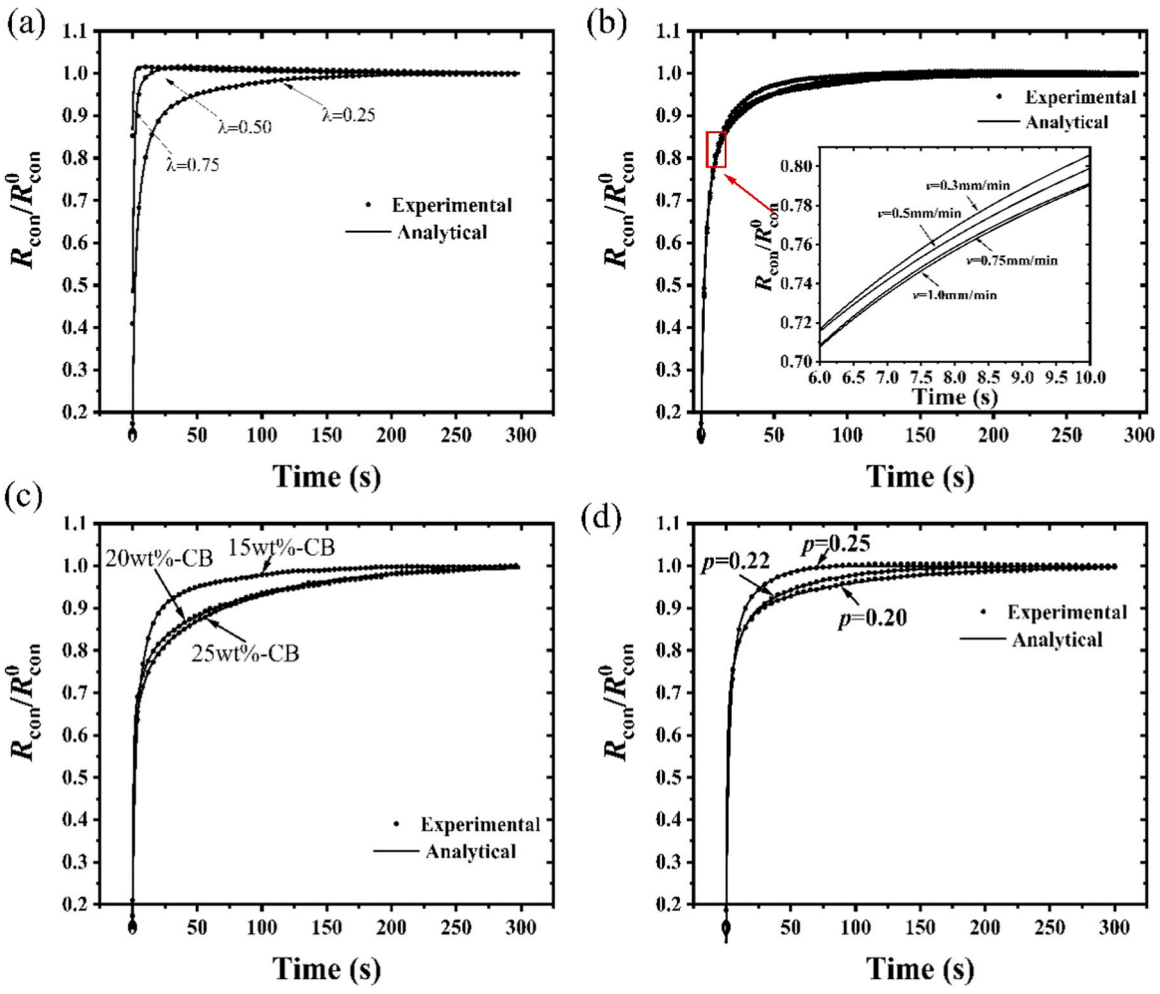

Fig. 9. Creep behaviors of contact resistance under releasing conditions. Experimental data and analytical line of creep contact resistance with compression amplitude (p = 0.25 and V_s= 9.5 v%) (**a**), compression speed (p = 0.25 and V_s= 9.5 v%) (**b**), CB content (p = 0.25) (**c**) and relative density (V_s= 9.5 v%) (**d**).

superior sensing capabilities, although it has limitations in accurately capturing the piezoresistive behavior of low pore-density materials, closed-pore materials, and 3D printed materials negative Poisson's ratio. The insights gained from this study can be utilized to enhance the piezoresistive properties of PPN-based sensors, leading to improved performance and reliability in various applications. The results of this study also suggest that overcoming the issue of molecular chain slippage within porous polymers and eliminating the resistance overshooting are crucial for PPN-based piezoresistive sensors. Future research directions could include exploring advanced functional matrices with low molecular chain slippage and high-temperature resistance, as well as advanced conductive networks to mitigate the issue of resistance overshooting.

CRediT authorship contribution statement

Zhang Jianpeng: Conceptualization, Formal analysis, Investigation, Methodology, Resources, Software, Writing – original draft. **Wang Ziya:** Data curation, Formal analysis, Methodology, Validation. **Shang Chao:** Data curation, Investigation, Methodology, Software. **Qian Zhengfang:** Formal analysis, Investigation, Methodology, Visualization, Writing – review & editing. **Wu Zhangming:** Conceptualization, Investigation, Visualization, Writing – review & editing. **Yu Xinge:** Investigation, Validation, Writing – review & editing. **Peng Zhengchun:** Formal analysis, Funding acquisition, Project administration, Resources, Supervision, Visualization, Writing – review & editing.

Declaration of Competing Interest

The authors declare that they have no known competing financial interests or personal relationships that could have appeared to influence the work reported in this paper.

Data availability

No data was used for the research described in the article.

Acknowledgments

This work was financially supported by the joint funding program of Guangdong Department of Science and Technology and Hongkong Innovation and Technology Fund under grant 2021A0505110015, and the Science and Technology Innovation Council of Shenzhen under grants KQTD20170810105439418, KQTD20180412181422399, and JCYJ20200109114237902.

Appendix A. Supporting information

Supplementary data associated with this article can be found in the online version at doi:10.1016/j.sna.2023.115002.

References

[1] X. Sun, C. Huang, L. Wang, L. Liang, Y. Cheng, W. Fei, et al., Recent progress in graphene/polymer nanocomposites, Adv. Mater. 33 (2021) 2001105.
[2] S. Wang, Y. Huang, E. Chang, C. Zhao, A. Ameli, H.E. Naguib, et al., Evaluation and modeling of electrical conductivity in conductive polymer nanocomposite foams with multiwalled carbon nanotube networks, Chem. Eng. J. 411 (2021) 128382.
[3] X. Lü, T. Yu, F. Meng, W. Bao, Wide-range and high-stability flexible conductive graphene/thermoplastic polyurethane foam for piezoresistive sensor applications, Adv. Mater. Technol. 6 (2021) 2100248.
[4] Q. Chen, Q. Gao, X. Wang, D.W. Schubert, X. Liu, Flexible, conductive, and anisotropic thermoplastic polyurethane/polydopamine /MXene foam for piezoresistive sensors and motion monitoring, Compos. Part A: Appl. Sci. Manuf. 155 (2022) 106838.
[5] T. Zhai, L. Verdolotti, S. Kacilius, P. Cerruti, G. Gentile, H. Xia, et al., High piezo-resistive performances of anisotropic composites realized by embedding rGO-based chitosan aerogels into open-cell polyurethane foams, Nanoscale 11 (2019) 8835–8844.
[6] Z. Wu, P. Wang, B. Zhang, H. Guo, C. Chen, Z. Lin, et al., Highly durable and easily integrable triboelectric foam for active sensing and energy harvesting applications, Adv. Mater. Technol. 6 (2021) 2000737.
[7] Z. Peng, J. Zhang, S. Wei, C. Liu, C. Shang, Z. He, et al., Porous nanocomposites with enhanced intrinsic piezoresistive sensitivity for a highly integrated multimodal tactile sensor, (2023).
[8] L. Sorrentino, M. Aurilia, S. Iannace, Polymeric foams from high-performance thermoplastics, Adv. Polym. Technol. 30 (2011) 234–243.
[9] L.M. Matuana, C.A. Diaz, Study of cell nucleation in microcellular poly(lactic acid) foamed with supercritical CO_2 through a continuous-extrusion, Process, Ind. Eng. Chem. Res. 49 (2010) 2186–2193.
[10] C.B. Park, D.F. Baldwin, N.P. Suh, Effect of the pressure drop rate on cell nucleation in continuous processing of microcellular polymers, Polym. Eng. Sci. 35 (1995) 432–440.
[11] Y. Ding, T. Xu, O. Onyilagha, H. Fong, Z. Zhu, Recent advances in flexible and wearable pressure sensors based on piezoresistive 3D monolithic conductive sponges, ACS Appl. Mater. Interfaces 11 (2019) 6685–6704.
[12] S. Wu, J. Zhang, R.B. Ladani, A.R. Ravindran, A.P. Mouritz, A.J. Kinloch, et al., Novel electrically conductive porous PDMS/carbon nanofiber composites for deformable strain sensors and conductors, ACS Appl. Mater. Interfaces 9 (2017) 14207–14215.
[13] W. Zhao, Z. Wang, J. Zhang, X. Wang, Y. Xu, N. Ding, et al., Vat photopolymerization 3D printing of advanced soft sensors and actuators: from architecture to function, Adv. Mater. Technol. 6 (2021) 2001218.
[14] S. Araby, B. Philips, Q. Meng, J. Ma, T. Laoui, C.H. Wang, Recent advances in carbon-based nanomaterials for flame retardant polymers and composites, Compos. Part B: Eng. 212 (2021) 108675.
[15] W. Zhang, S. Kang, X. Liu, B. Lin, Y. Huang, Experimental study of a composite beam externally bonded with a carbon fiber-reinforced plastic plate, J. Build. Eng. 71 (2023) 106522.
[16] M. Li, Q. Guo, L. Chen, L. Li, H. Hou, Y. Zhao, Microstructure and properties of graphene nanoplatelets reinforced AZ91D matrix composites prepared by electromagnetic stirring casting, J. Mater. Res. Technol. 21 (2022) 4138–4150.
[17] V. Goodarzi, M. Kokabi, M. Razzaghi Kashani, A. Reza Bahramian, Prediction of long-term mechanical properties of PVDF/BaTiO3 nanocomposite, J. Appl. Polym. Sci. 131 (2014).
[18] V. Nassiet, B. Hassoune-Rhabbour, O. Tramis, J.-A. Petit, 22 - Electrical and electronics, in: R.D. Adams (Ed.) Adhesive Bonding (Second Edition), Woodhead Publishing2021, pp. 719–61.
[19] A. Sanli, A. Benchirouf, C. Müller, O. Kanoun, Piezoresistive performance characterization of strain sensitive multi-walled carbon nanotube-epoxy nanocomposites, Sens. Actuators A: Phys. 254 (2017) 61–68.
[20] J. Tolvanen, J. Hannu, H. Jantunen, Hybrid foam pressure sensor utilizing piezoresistive and capacitive sensing mechanisms, IEEE Sens. J. 17 (2017) 4735–4746.
[21] W. Klimm, K. Kwok, Computational analysis of tunneling conduction in piezoresistive carbon nanotube polymer composites, J. Intell. Mater. Syst. Struct. 34 (2022) 928–943.
[22] W. Klimm, K. Kwok, Tunneling resistance model for piezoresistive carbon nanotube polymer composites, Nanotechnology 34 (2023) 045502.
[23] J. Zhang, Z. Wang, Z. Peng, Analytical model of the piezoresistive behavior of highly compressible sensors made of microporous nanocomposites, Adv. Theory Simul. 4 (2021) 2100247.
[24] M. Soldatov, H. Liu, Hybrid porous polymers based on cage-like organosiloxanes: synthesis, properties and applications, Prog. Polym. Sci. 119 (2021) 101419.
[25] M. Rostamian, H. Hosseini, V. Fakhri, P.Y. Talouki, M. Farahani, A.J. Gharehtzpeh, et al., Introducing a bio sorbent for removal of methylene blue dye based on flexible poly(glycerol sebacate)/chitosan/graphene oxide ecofriendly nanocomposites, Chemosphere 289 (2022) 133219.
[26] V. Fakhri, A. Jafari, M.A. Shafiei, M.V. Ehteshamfar, S. Khalighiyan, H. Hosseini, et al., Development of physical, mechanical, antibacterial and cell growth properties of poly(glycerol sebacate urethane) (PGSU) with helping of curcumin and hydroxyapatite nanoparticles, Polym. Chem. 12 (2021) 6263–6282.
[27] H. Golbaten-Mofrad, A. Seyfi Sahzabi, S. Seyfikar, M.H. Salehi, V. Goodarzi, F. R. Wurm, et al., Facile template preparation of novel electroactive scaffold composed of polypyrrole-coated poly(glycerol-sebacate-urethane) for tissue engineering applications, Eur. Polym. J. 159 (2021) 110749.
[28] Z. Wang, X. Guan, H. Huang, H. Wang, W. Lin, Z. Peng, Full 3D printing of stretchable piezoresistive sensor with hierarchical porosity and multimodulus architecture, Adv. Funct. Mater. 29 (2019) 1807569.
[29] S. Kumar, T.K. Gupta, K.M. Varadarajan, Strong, stretchable and ultrasensitive MWCNT/TPU nanocomposites for piezoresistive strain sensing, Compos. Part B: Eng. 177 (2019) 107285.
[30] L. Yang, Y. Liu, C.D.M. Filipe, D. Ljubic, Y. Luo, H. Zhu, et al., Development of a highly sensitive, broad-range hierarchically structured reduced graphene oxide/polyHIPE foam for pressure sensing, ACS Appl. Mater. Interfaces 11 (2019) 4318–4327.
[31] W. Klimm, K. Kwok, Mechanism of resistance relaxation and hysteresis in viscoelastic piezoresistive polymer nanocomposites, Int. J. Mech. Mater. Des. 18 (2022) 769–783.
[32] B. Fazekas, T.J. Goda, Determination of the hyper-viscoelastic model parameters of open-cell polymer foams and rubber-like materials with high accuracy, Mater. Des. 156 (2018) 596–608.
[33] Z.-H. Tang, Y.-Q. Li, P. Huang, H. Wang, N. Hu, S.-Y. Fu, Comprehensive evaluation of the piezoresistive behavior of carbon nanotube-based composite strain sensors, Compos. Sci. Technol. 208 (2021) 108761.
[34] K. Bicy, D. Rouxel, M. Poncot, I. Royaud, P. Bourson, D. Chapron, et al., Interfacial tuning and designer morphologies of microporous membranes based on polypropylene/natural rubber nanocomposites, J. Appl. Polym. Sci. 138 (2021) 51208.
[35] Q. Suo, J. Zhang, J. Cheng, L. Shi, Preparation, microstructure, and piezoresistive behavior of conductive nanocomposite foams based on poly(1-butene) and carbon black, Appl. Phys. A 123 (2016) 54.
[36] H. Liu, M. Dong, W. Huang, J. Gao, K. Dai, J. Guo, et al., Lightweight conductive graphene/thermoplastic polyurethane foams with ultrahigh compressibility for piezoresistive sensing, J. Mater. Chem. C. 5 (2017) 73–83.
[37] M. Nagrath, A. Alhalawani, A. Rahimnejad Yazdi, M.R. Towler, Bioactive glass fiber fabrication via a combination of sol-gel process with electro-spinning technique, Mater. Sci. Eng.: C. 101 (2019) 521–538.
[38] R. Ghamarpoor, M. Jamshidi, Synthesis of vinyl-based silica nanoparticles by sol–gel method and their influences on network microstructure and dynamic mechanical properties of nitrile rubber nanocomposites, Sci. Rep. 12 (2022) 15286.
[39] X. Du, M. Dehghani, N. Alsaadi, M.G. Nejad, S. Saber-Samandari, D. Toghraie, et al., A femoral shape porous scaffold bio-nanocomposite fabricated using 3D printing and freeze-drying technique for orthopedic application, Mater. Chem. Phys. 275 (2022) 125302.
[40] M.A. Mudassir, H.Z. Aslam, T.M. Ansari, H. Zhang, I. Hussain, Fundamentals and design-led synthesis of emulsion-templated porous materials for environmental applications, Adv. Sci. 8 (2021) 2102540.
[41] C. Wang, M.J. Park, D.H. Seo, E. Drioli, H. Matsuyama, H. Shon, Recent advances in nanomaterial-incorporated nanocomposite membranes for organic solvent nanofiltration, Sep. Purif. Technol. 268 (2021) 118657.
[42] S. Wang, Y. Huang, C. Zhao, E. Chang, A. Ameli, H.E. Naguib, et al., Theoretical modeling and experimental verification of percolation threshold with MWCNTs' rotation and translation around a growing bubble in conductive polymer composite foams, Compos. Sci. Technol. 199 (2020) 108345.
[43] X. Guan, Z. Wang, W. Zhao, H. Huang, S. Wang, Q. Zhang, et al., Flexible piezoresistive sensors with wide-range pressure measurements based on a graded nest-like architecture, ACS Appl. Mater. Interfaces 12 (2020) 26137–26144.
[44] A. Soranno, F. Zosel, H. Hofmann, Internal friction in an intrinsically disordered protein—Comparing Rouse-like models with experiments, J. Chem. Phys. 148 (2018) 123326.
[45] M. Hossain, A.F.M.S. Amin, M.N. Kabir, Eight-chain and full-network models and their modified versions for rubber hyperelasticity: a comparative study, 24(2015) 11–24.
[46] T.A. Ezquerra, M. Kulescza, C.S. Cruz, F.J. Baltá-Calleja, Charge transport in polyethylene–graphite composite materials, Adv. Mater. 2 (1990) 597–600.
[47] G.E. Archie, The Electrical Resistivity Log as an Aid in Determining Some Reservoir Characteristics, Trans. AIME 146 (1942) 54–62.
[48] D. Mercier, V. Mandrillon, A. Holtz, V. Fabien, M. Verdier, Y. Bréchet, Quantitative Evolution of Electrical Contact Resistance between Aluminum Thin Films 2012.
[49] F. Tanaka, Polymer Physics: Applications to Molecular Association and Thermoreversible Gelation, Cambridge, Cambridge University Press, 2011.
[50] W.Y. Zhao, Z.Y. Wang, J.P. Zhang, X.P. Wang, Y.T. Xu, N. Ding, et al., Vat Photopolymerization 3D Printing of Advanced Soft Sensors and Actuators: From Architecture to Function, Adv. Mater. Technol. 6 (2021) 31.
[51] P.Y. Talouki, S.H. Tackallou, S. Shojaei, S.Z. Benisi, V. Goodarzi, The role of three-dimensional scaffolds based on polyglycerol sebacate/ polycaprolactone/ gelatin in the presence of Nanohydroxyapatite in promoting chondrogenic differentiation of human adipose-derived mesenchymal stem cells, Biol. Proced. Online 25 (2023) 9.
[52] V. Faghihi-Rezaei, H.A. Khonkdar, V. Goodarzi, G. Darbemamieh, M. Otadi, Design and manufacture of 3D-cylindrical scaffolds based on PLA/TPU/n-HA with the help of dual salt leaching technique suggested for use in cancellous bone tissue engineering, J. Biomater. Sci., Polym. Ed. 34 (2023) 1430–1452.
[53] K. Yang, N. Qin, H. Yu, C. Zhou, H. Deng, W. Tian, et al., Correlating multi-scale structure characteristics to mechanical behavior of Caprinae horn sheaths, J. Mater. Res. Technol. 21 (2022) 2191–2202.
[54] M. Zhang, X. Jiang, M. Arefi, Dynamic formulation of a sandwich microshell considering modified couple stress and thickness-stretching, Eur. Phys. J. 138 (2023) 227.

[55] J.J. ZHAO Yuhong, C.H.E.N. Liwen, X.U. Fanghong, H.O.U. Hua, Current Research Status of Interface of Ceramic-Metal Laminated Composite Material for Armor Protection, Acta Met. Sin. 57 (2021) 1107–1125.
[56] S. Zhao, D. Lou, G. Li, Y. Zheng, G. Zheng, K. Dai, et al., Bridging the segregated structure in conductive polypropylene composites: An effective strategy to balance the sensitivity and stability of strain sensing performances, Compos. Sci. Technol. 163 (2018) 18–25.
[57] B. Zhang, B. Li, S. Jiang, Poly(phenylmethylsiloxane) functionalized multiwalled carbon nanotube/poly(dimethylsiloxane) nanocomposites with high piezoresistivity, low modulus and high conductivity, J. Mater. Sci.: Mater. Electron. 28 (2017) 6897–6906.
[58] J.-X. Lin, G. Chen, H.-s Pan, Y.-c Wang, Y.-c Guo, Z.-x Jiang, Analysis of stress-strain behavior in engineered geopolymer composites reinforced with hybrid PE-PP fibers: A focus on cracking characteristics, Compos. Struct. 323 (2023) 117437.
[59] S. Zhou, C. Lu, X. Zhu, F. Li, Preparation and characterization of high-strength geopolymer based on BH-1 lunar soil simulant with low alkali content, Engineering 7 (2021) 1631–1645.
[60] K. Yang, H. Yu, X. Cao, J. Guan, S. Cai, Z. Yang, et al., The critical role of corrugated lamellae morphology on the tough mechanical performance of natural Syncerus caffer horn sheath, Cell Reports Physical, Science (4() (2023).
[61] S. Zhu, X. Li, Y. Bian, N. Dai, J. Yong, Y. Hu, et al., Inclination-enabled generalized microfluid rectifiers via anisotropic slippery hollow tracks, Adv. Mater. Technol. 8 (2023) 2300267.
[62] W. Li, X.-s Chu, F. Wang, Y.-y Dang, X.-y Liu, X.-c Wang, et al., Enhanced cocatalyst-support interaction and promoted electron transfer of 3D porous g-C3N4/GO-M (Au, Pd, Pt) composite catalysts for hydrogen evolution, Appl. Catal. B: Environ. 288 (2021) 120034.
[63] L. Sun, T. Liang, C. Zhang, J. Chen, The rheological performance of shear-thickening fluids based on carbon fiber and silica nanocomposite, Phys. Fluids 35 (2023) 032002.
[64] W. Liu, H. Zhou, S. Zhang, C. Zhao, Variable parameter creep model based on the separation of viscoelastic and viscoplastic deformations, Rock. Mech. Rock. Eng. 56 (2023) 4629–4645.

Dr. Jianpeng Zhang is a postdoctoral researcher in Solid Mechanics, specializing in flexible structural mechanics and their applications in soft wearable devices. Holding a Ph. D. in Solid Mechanics from Beihang University, Dr. Zhang brings over a decade of research experience in nanotechnology and has actively contributed to several groundbreaking projects in electronic skin (E-skin) and smart sensors.

Dr. Ziya Wang is currently an assistant professor of Physics and Optoelectronic Engineering at Shenzhen University. She received her B.S. and Ph.D. degrees in physics from the University of Science & Technology Beijing. Her research interests are in smart functional materials, soft sensors and electronics, and robotic tactile perception.

Dr. Chao Shang received a Ph.D. degree in condensed matter physics from the University of Science and Technology of China, Hefei, China, in 2019. He is currently working as a Postdoctoral researcher at the School of Physics and Optoelectronic Engineering, Shenzhen University, Shen Zhen, China. His research interests include hydrogel, additive manufacturing, electronic skin, and deep learning

Prof. Zhengfang Qian is a distinguished professor in the School of Physics and Optoelectronic Engineering at Shenzhen University. He has held positions at leading institutions like the Chinese Academy of Sciences, several U.S. universities, and prominent companies including Motorola and Smart Technologies. During his career, he has led numerous major projects in China and the U.S., securing over $10 million in project funding. His expertise spans various fields, from engineering materials and electronics to wireless communication technologies.

Prof. Zhangming Wu is a Senior Lecturer at Cardiff University's School of Engineering. His research focuses on mechanics, modeling, and optimization. He has developed extensive expertise in mathematical modeling, optimization, thin-walled structures, and smart sensing systems, contributing significantly to the fields of mechanical, sustainable transport, civil engineering, and biomedical engineering.

Prof. Xinge Yu is an Associate Professor in the Department of Biomedical Engineering at the City University of Hong Kong. He specializes in flexible electronics and bio-electronics. His research primarily focuses on three critical areas: developing and engineering functional materials, designing and fabricating devices for sensing, control, and actuation across various scales, and integrating and optimizing system-level electronics. These efforts are directed towards the creation of innovative bio-integrated electronics for diverse applications.

Prof. Zhengchun Peng is a distinguished professor in the School of Physics and Optoelectronic Engineering at Shenzhen University. His research interest mainly lies in flexible/stretchable electronics, micro/nano sensors and actuators, and their applications in robotic e-skin, health monitoring, and brain-machine interface. In particular, he focuses on novel material synthesis, innovative device design, and advanced micro/nano fabrication, in order to creating flexible sensors, actuators, and memory devices capable of bending, stretching, or reconfiguring with mechanical deformation, while maintaining excellent electronic performance.